Novel Cu^{III} Bis-1,2-dichalcogenene Complexes with Tunable 3D Framework through Alkaline Cation Coordination: A Structural and Theoretical Study

Xavi Ribas,[a] João C. Dias,[b] Jorge Morgado,[b, c] Klaus Wurst,[d] Elies Molins,[a] Eliseo Ruiz,[e] Manuel Almeida,[b] Jaume Veciana,[a] and Concepció Rovira*[a]

Abstract: The deprotonated form of the ligands pyrazine-2,3-diselenol (pds) and pyrazine-2,3-dithiol (pdt) react with $Cu(ClO_4)_2 \cdot 6H_2O$ to form different Cu^{III} complexes $Na[Cu^{III}(pds)_2] \cdot 2H_2O$ (**1**), $Li[Cu^{III}(pds)_2] \cdot 3H_2O$ (**2**), and $Na[Cu^{III}(pdt)_2] \cdot 2H_2O$ (**4**) depending on the countercation compound used as deprotonating agent (NaOH, LiOH). Two other Cu^{III} complexes were obtained by replacement of the alkali metal cations with tetrabutylammonium (TBA^+), namely, $TBA[Cu^{III}(pds)_2]$ (**3**), and $TBA[Cu^{III}(pdt)_2]$ (**5**). All complexes were characterized by ^1H and ^{13}C NMR and IR spectroscopy, electronic absorption, elemental analysis, cyclic voltammetry (CV), and X-ray crystallography. Electrical conductivity measurements on single crystals show that these salts exhibit insulating behavior. The crystal structure of these species revealed a lateral coordination capability of the N atoms of the pyrazine ring of both pds and pdt ligands towards the alkali metal ions, which leads to the build up of a net of coordinative bonds, hydrogen bonds, and contacts that result in the final 3D structure. Two parameters control the crystal engineering of the final 3D structures: the nature of the alkali metal countercation and the nature of the chalcogen atom (Se/S), which allow fine-tuning of complex 3D crystal lattice. Density functional calculations were performed on the $[Cu(pds)_2]$ and $[Cu(pdt)_2]$ systems to investigate the electronic structure of the complexes and understand their electronic and electrochemical behavior by studying the frontier molecular orbitals. This study also reveals whether the redox processes take place on the ligands or on the metal center, a question under continuous discussion in the literature.

Keywords: alkali metals · copper · crystal engineering · density functional calculations · dichalcogenate ligands

Introduction

Square-planar transition-metal dithiolene complexes are widely used as building blocks in the synthesis of molecular conductor materials,[1] and some examples showing metallic and superconducting properties have been described.[2] The versatility of their oxidation states confers on them different magnetic moments that depend on the nature of the metal atom. These compounds usually crystallize by forming stacks of complexes, which give rise to quasi-one-dimensional electronic systems. The major problem associated with these systems is their instability at low temperatures due to a metal-to-insulator transition caused by the Peierls distortion,[3] which prevents the appearance of superconductivity. It has been suggested that this distortion can be suppressed at low temperatures by increasing the electronic dimensionality of the systems. Two strategies have been employed for this purpose: increasing the number of peripheral sulfur atoms associated with the ligand framework to strengthen the intermolecular interactions through more S···S contacts, and changing from sulfur ligands to selenium analogues.[4] The greater spatial extension of the Se 4d orbitals compared

[a] Dr. X. Ribas, Prof. E. Molins, Prof. J. Veciana, Prof. C. Rovira
Institut de Ciencia de Materials de Barcelona
CSIC, Campus de la UAB, 08193 Bellaterra (Spain).
Fax: (+34) 935-805729.
E-mail: cun@icmab.es

[b] J. C. Dias, Prof. J. Morgado, Prof. M. Almeida
Departamento de Química, Instituto Tecnológico e Nuclear
2686-953 Sacavém, (Portugal)

[c] Prof. J. Morgado
Departamento de Engenharia Química, Instituto Superior Tecnico,
Av. Rovisco Pais, 1049-001 Lisboa (Portugal)

[d] Dr. K. Wurst
Institut für Allgemeine Anorganische und Theoretische Chemie
Universiat Innsbruck, Innrain 52a, Innsbruck (Austria)

[e] Dr. E. Ruiz
Departament de Química Inorgànica
Universitat de Barcelona, Av. Diagonal 647
08028 Barcelona (Spain)

Supporting information for this article is available on the WWW under http://www.chemeurj.org or from the author, including average interatomic aromatic ring distances and chalcogen–chalcogen distances (Table S1), optimized bond lengths and angles for dianionic $[Cu(pds)_2]^{2-}$, monoanionic $[Cu(pds)_2]^-$, neutral $[Cu(pds)_2]$ and monoanionic $[Cu(pdt)_2]^-$ obtained from DFT calculations with the B3LYP functional (Tables S2 and S3).

 DOI: 10.1002/chem.200305422

to the S 3d orbitals is expected to increase the interaction in the complexes and lead not only to increased dimensionality but also to higher electrical conductivity.[5]

In spite of more than three decades of studies, the description of the electronic structure of transition-metal dithiolene complexes is still a matter of ongoing debate in the literature.[6,7] We focus our attention on the subfamily of transition-metal complexes containing two bidentate *ortho*-disubstituted aromatic ligands bearing O, N, S, Se, or a combination thereof as coordinating atoms (Scheme 1).[8–17] The rich electrochemical behavior of the latter group of complexes opens the question whether the redox processes are ligand- or metal-centered. Experimental and theoretical evidence has been reported on de-aromatization of the benzene rings to give an open-shell *o*-semiquinonate type ligand, and the singlet diradical ground states of some neutral complexes have been characterized (Schemes 1 and 2).[13] Thus, the contribution of the ligands to the HOMO and their role upon oxidation of the complex, often referred as innocent or noninnocent character of the ligands, is still under discussion. Many different dithiolene-type ligands have been studied, but only a small amount of work was devoted to Se-containing ligands. An *o*-iminoselenobenzosemiquinonato π radical was described in a recent paper.[17]

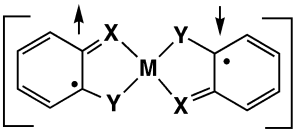

(X,Y) = (NH,NH); (NH,O); (O,O); (S,S); (S, NH)

M = $Ni^{(II)}$, $Pd^{(II)}$, $Pt^{(II)}$

Scheme 1. Singlet diradical ground states of complexes $[ML_2]$ (M = Ni, Pd, Pt).[12]

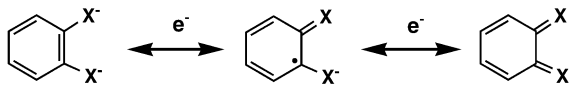

o-catecholate *o*-semiquinonate *o*-quinone

Scheme 2. Reversible oxidation states for ligands with *ortho*-disubstituted aromatic rings (X = O, NH, S).

In this context, here we present the synthesis of four new copper(III) complexes of the aromatic ligands pyrazine-2,3-diselenolate (pds^{2-}) and pyrazine-2,3-dithiolate (pdt^{2-}) that, from the point of view of forming new materials, have an additional possibility of increasing the dimensionality through the N atoms in the pyrazine ring. Differences in 3D supramolecular organization of the complexes in the crystal lattice that depend on the countercation used (alkali metal or TBA ions) and on the chalcogen atom present in the ligand were found and will be discussed. We also discuss the open- or closed-shell character of the aromatic ligands pds and pdt in our copper complexes on the basis of experimental and theoretical data. These ligands represent a new group of aromatic (pyrazine versus benzene rings) *ortho*-disubstituted ligands with Se or S as coordinating atoms that broaden the scope for the electronic description of related systems.

Abstract in Catalan: *Els lligands pirazina-2,3-diselenol (pds) i pirazina-2,3-ditiol (pdt), en la seva forma desprotonada, reaccionen amb $Cu(ClO_4)_2{\cdot}6H_2O$ per a formar diferents complexes de Cu^{III}, $Na[Cu^{III}(pds)_2]{\cdot}2H_2O$ (**1**), $Li[Cu^{III}(pds)_2]{\cdot}3H_2O$ (**2**) i $Na[Cu^{III}(pdt)_2]{\cdot}2H_2O$ (**4**), depenent de la base usada com a agent desprotonant (NaOH, LiOH). S'han obtingut dos complexes de Cu^{III} més per substitució dels cations alcalins pel catió tetrabutilamoni (TBA^+), $TBA[Cu^{III}(pds)_2]$ (**3**) i $[Cu^{III}(pdt)_2]TBA$ (**5**). Tots els complexes han estat caracteritzats mitjançant ^1H i ^{13}C RMN, espectroscòpia d'infrarojos, absorció electrònica, anàlisi elemental, estudis de Voltametria Cíclica (VC) i cristal·lografia de Raigs-X. També s'han realitzat mesures de conductivitat elèctrica en monocristalls de les sals estudiades, mostrant un comportament aïllant en tots els casos. L'estructura cristal·lina d'aquests compostos ha permés estudiar la capacitat dels atoms de N dels anells de pirazina, en ambdós lligands pds i pdt, per a presentar una coordinació lateral amb els ions alcalins, de manera que es construeix una xarxa d'enllaços de coordinació, d'enllaços d'hidrogen i de contactes que donen lloc finalment a l'estructura tridimensional dels compostos. Existeixen dos paràmetres que controlen el fenomen d'enginyeria cristal·lina en les estructures 3D finals: la naturalesa del contracatió alcalí i la naturalesa de l'àtom calcogen (Se/S). La seva modificació permet el control minuciós de la xarxa cristal·lina 3D dels complexes. S'han realitzat càlculs DFT en els sistemes $Cu(pds)_2$ and $Cu(pdt)_2$ amb l'objectiu d'investigar l'estructura electrònica dels complexes i entendre el seu comportament electrònic i electroquímic a través de L'estudi dels corresponents orbitals moleculars frontera. Aquest estudi també permet saber si els processos redox tenen lloc sobre els lligands o sobre el metall, una qüestió en contínua discussió en la bibliografia.*

Results

Synthesis: Pyrazine-2,3-diselenol (pds) and pyrazine-2,3-dithiol (pdt) were prepared by literature procedures.[18] The general procedure for the synthesis of $[Cu(pds)_2]^-$ and $[Cu(pdt)_2]^-$ salts is depicted in Scheme 3. The lithium salt of the pds complex was prepared by following the procedure reported for the synthesis of $Na[Cu^{III}(pds)_2]{\cdot}2H_2O$ (**1**).[19] Thus, the diselenolate formed by treatment of pds with aqueous LiOH was treated with $Cu(ClO_4)_2{\cdot}6H_2O$ to give the corresponding red-colored Cu^{II} complex, which was oxidized with a stream of air to give dark green $Li[Cu^{III}(pds)_2]{\cdot}3H_2O$ (**2**). $TBA[Cu^{III}(pds)_2]$ (**3**) was obtained by cation exchange of **1** or **2** with an excess of TBABr. The sulfur analogue $Na[Cu^{III}(pdt)_2]{\cdot}2H_2O$ (**4**) was prepared similarly to **1** and **2**, but instead of air, addition of I_2 (a stronger oxidant) was required to obtain the Cu^{III} complex in good yield.

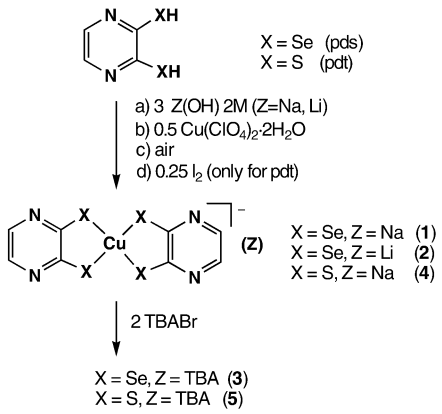

Scheme 3. Synthesis of complexes **1**–**5**.

TBA[$Cu^{III}(pds)_2$] (**5**) was prepared by following the same methodology as for **3**.

Characterization: Complexes **1**–**5** were characterized by NMR, UV/Vis, and IR spectroscopy, elemental analysis, X-ray crystallography, cyclic voltammetry (CV), and electrical conductivity measurements.

The ^{1}H NMR spectra show a single narrow peak, at $\delta =$ 8.16 ppm for complexes **1**–**3** and at $\delta = 8.13$ ppm for **4** and **5**, corresponding to the four aromatic pyrazine protons of the pds and pdt moieties, respectively. The diamagnetic behavior of the complexes agrees with a Cu^{III} oxidation state in a square-planar geometry leading to a d^8 electronic configuration. Indeed, the Cu^{II}/Cu^{III} redox couple appears in the cyclic voltammogram as a quasireversible wave at $E_{1/2} = -0.54$ V for **1** and **3**, -0.52 V for **2**, -0.30 V for **4**, and -0.33 V for **5**. The very low potentials of the redox processes in these Cu compounds (especially **1**–**3**), show the capability of the pyrazine dichalcogenate ligands to stabilize the +3 oxidation state of the Cu center. This hypothesis is supported by the observation that complexes **1** and **2** are simply obtained by air oxidation of the corresponding red Cu^{II} species. Although complex **4** can also be obtained by air oxidation, the yield is very poor, and therefore the addition of a stronger oxidant such as I_2 is mandatory to obtain the desired Cu^{III} species in good yield.

The UV/Vis/NIR spectra of **1**–**3** and **5** in CH_3CN and of **4** in acetone show an intense band at about 380 nm ($\varepsilon \approx$ 40 000–50 000 $cm^{-1}M^{-1}$) and weaker bands in the visible and near-infrared region at 536 nm (650 $cm^{-1}M^{-1}$) and 1020 nm (195 $cm^{-1}M^{-1}$) for **4** and **5**, and at 596 nm (950 $cm^{-1}M^{-1}$) and 920 nm (120 $cm^{-1}M^{-1}$) for **1**–**3**. The shifts observed in the absorption band when Se is replaced by S are discussed in the next section.

Electrical conductivity measurements on single crystals of complexes **1, 2**, and **4**, in which well-segregated stacks of complexes are observed, revealed insulating behavior, with $\sigma_{RT} < 10^{-6}$ S cm^{-1} in all cases.

Structural analysis

*Li[$Cu^{III}(pds)_2$]·3 H_2O (**2**)*: Complex **2** was characterized as a square-planar Cu^{III} complex by NMR spectroscopy and X-ray diffraction (see Table 1 for crystal data) on a black needle-shaped single crystal obtained by slow diffusion of diethyl ether into a solution of the compound in acetonitrile.

The asymmetric unit contains two pds ligands, one Li atom, three water molecules in general positions, and two half Cu atoms located at symmetry centers. The ORTEP plot of the anion [$Cu^{III}(pds)_2$]$^-$ (Figure 1) shows a square-planar geometry around the Cu center for the two crystallographically independent complex units, in one of which the N1 atom of each pds moiety is coordinated to a Li atom, whereas in the second complex unit, the N3 and N4 atoms exhibit short contacts with water molecules. All Cu–Se bond lengths are close to 2.30 Å (see Table 2). However, as shown in Figure 1, a small distortion is observed in the planarity of the complex in which Li is coordinated to the pds moieties:

Table 1. Crystal data and structure refinement of complexes **1**–**5**.

	Na[$Cu^{III}(pds)_2$]·2 H_2O (**1**)[b]	Li[$Cu^{III}(pds)_2$]·3 H_2O (**2**)	TBA[$Cu^{III}(pds)_2$] (**3**)	Na[$Cu^{III}(pdt)_2$] ·2 H_2O (**4**)	TBA[$Cu^{III}(pdt)_2$] (**5**)
formula	$C_8H_8CuN_4NaO_2Se_4$	$C_8H_{10}CuN_4LiO_3Se_4$	$C_{24}H_{40}CuN_5Se_4$	$C_8H_8CuN_4NaO_2S_4$	$C_{24}H_{40}CuN_5S_4$
M_r	594.55	596.52	777.99	406.95	590.39
crystal system	monoclinic	monoclinic	monoclinic	monoclinic	monoclinic
space group	$P2_1/c$	$P2_1/n$	$P2_1/c$	$P2_1/c$	$P2_1/c$
a [Å]	4.0446(2)	8.0852(2)	18.2338(5)	3.8400(2)	9.315(4)
b [Å]	15.7964(9)	15.3528(5)	9.8625(3)	15.4075(7)	18.816(6)
c [Å]	11.6721(6)	12.8314(4)	17.5144(4)	11.5400(9)	17.086(4)
β [°]	91.563(3)	90.232(2)	106.932(1)	92.600(4)	94.57(2)
V [Å^3]	745.45(7)	1592.75(8)	3013.10(14)	682.06(7)	2985.2(17)
Z	2	4	4	2	4
ρ_{calcd} [g cm^{-3}]	2.649	2.488	1.715	1.982	1.314
crystal size [mm]	0.40 × 0.12 × 0.08	0.40 × 0.20 × 0.20	0.40 × 0.20 × 0.10	0.15 × 0.06 × 0.04	0.5 × 0.32 × 0.29
T [K]	233(2)	243(2)	233(2)	233(2)	294(2)
$\lambda(Mo_{K\alpha})$ [Å]	0.71073	0.71073	0.71073	0.71073	0.71073
μ [mm^{-1}]	11.262	10.522	5.578	2.247	1.033
reflections collected	4047	8220	16 171	3094	5431
independent reflections	1452 ($R_{int} = 0.0585$)	2499 ($R_{int} = 0.0481$)	4723 ($R_{int} = 0.0780$)	956 ($R_{int} = 0.0517$)	5245 ($R_{int} = 0.0678$)
GOF on F^2	1.067	1.093	1.044	1.148	1.031
R/R_w[a]	0.0290/0.0644	0.0280/0.0683	0.0345/0.0797	0.0392/0.0733	0.0598/0.1597

[a] $R = \Sigma \mid F_o - F_c \mid / \Sigma F_o$, $R_w = \{\Sigma[w(F_o^2 - F_c^2)^2] / \Sigma[w(F_o^2)^2]\}^{1/2}$, where $w = 1/[\sigma^2\{F_o^2 + (aP)^2 + bP]$, $P = (F_o^2 + 2F_c^2)/3$, and a and b are constants given in the Supporting Information. [b] See complete crystallographic description in ref. [19].

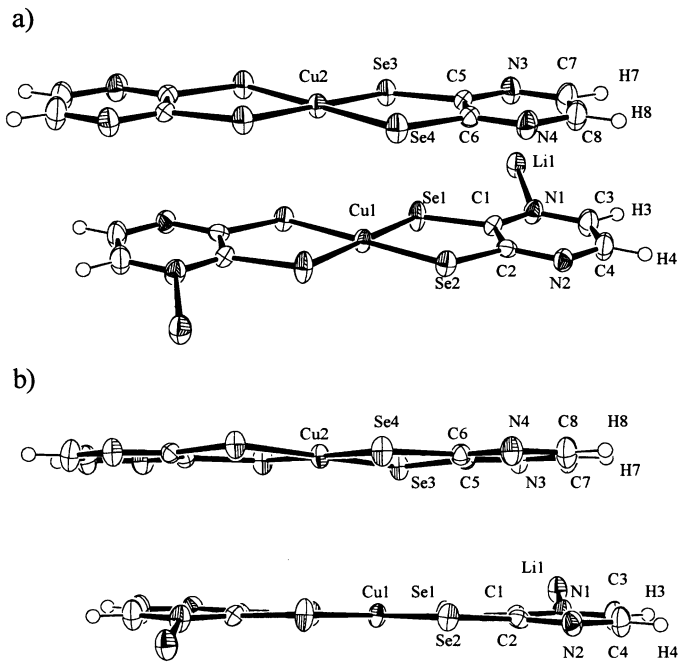

Figure 1. ORTEP plot of the stacked molecules of $Li[Cu^{III}(pds)_2]\cdot 3H_2O$ (**2**) in a lateral (a) and parallel (b) view to the $CuSe_4$ plane of the anion containing Cu1. Note that the two Li^+ are coordinated to only one complex.

both pyrazine rings are twisted in the same direction perpendicular to the long axis of the complex with respect to the $CuSe_4$ plane (torsion angle N-C-Se-Cu ca. 177°). This deviation from planarity can be explained by the coordination of the nitrogen atoms of the pyrazine rings to the Li^+ counterion and by the existence of short S···H–C contacts that twist the central and outer parts of the complex in opposite directions (similar to the sodium salt **1**).[19] In contrast, in the Li-free complex the rings are twisted in opposite directions parallel to the long axis of the complex with respect to the $CuSe_4$ plane, in the fashion of a chair conformation (torsion angle Se3-Cu2-Se4′-C6′ ca. 176°, see also Figure 2b).

As can be seen in Figure 2, the unit cell contains four $[Cu(pds)_2]^-$ units with their long axis roughly perpendicular to each other in a packing similar to that found in the corresponding Na compound **1**.[19] The Li-coordinated and uncoordinated anionic complexes alternate along the *a* axis to form tilted regular stacks with an average distance between stacked units of 3.6 Å. The angle between the stacking axis *a* and the average $Cu(pds)_2$ plane is 27° for Li-coordinated units and 30° for the noncoordinating units. In the stacks, Li-coordinated and uncoordinated complexes are skewed with lateral offset values of about 1.1 Å for the long axis of the complex and about 2.1 and 0.7 Å for the short axis (taking into consideration the skewed packing), as shown in Figure 2b and c.

In contrast to the octahedrally coordinated Na atoms (two N and four O atoms) in salt **1**, the lithium ions in **2** are

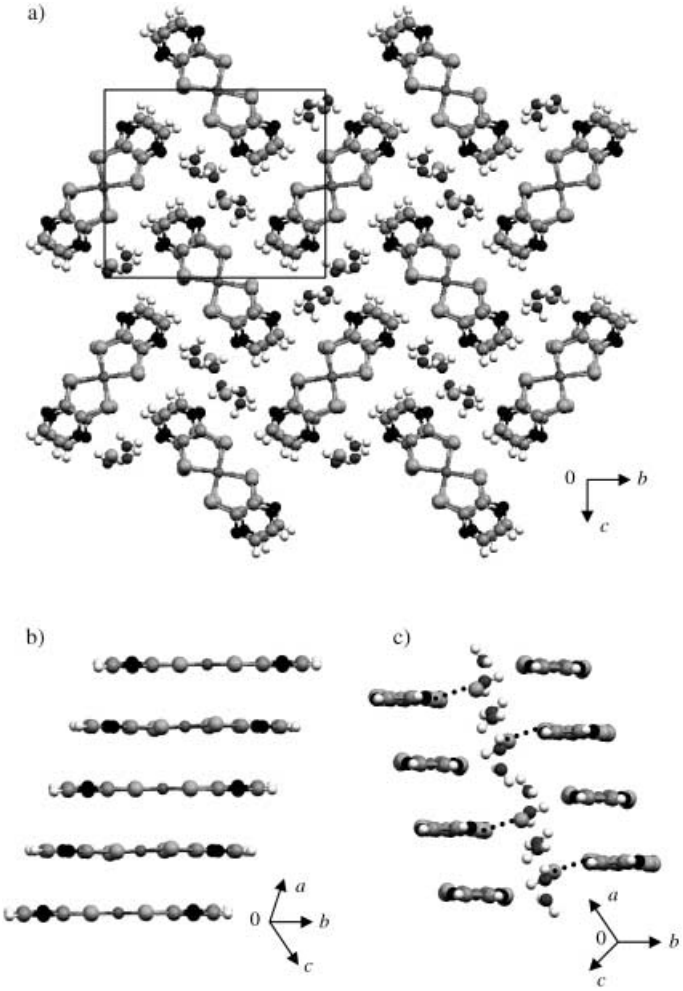

Figure 2. Crystal structure of $Li[Cu^{III}(pds)_2]\cdot 3H_2O$ (**2**). a) View along the stacking axis *a*. b) Stack of complex units viewed along the shortest axis of the complex. c) Parallel stacks of anions viewed along the longest axis with alternating Li coordination.

Table 2. Selected bond bengths [Å] and angles [°] for $Li[Cu^{III}(pds)_2]\cdot 3H_2O$ (**2**).

Cu1–Se1	2.2990(5)	Cu2–Se3	2.2991(5)
Cu1–Se2	2.3086(5)	Cu2–Se4	2.3066(5)
Se1–C1	1.887(5)	Se3–C5	1.895(5)
Se2–C2	1.882(5)	Se4–C6	1.879(5)
Li1–N1	2.131(10)	Li1–O1	1.946(11)
Li1–O2	1.957(10)	Li1–O3	1.900(11)
Cu1···Cu2	4.0426(2)	Li1-Li1′	4.619(20)
Se1-Cu1-Se1′	180	Se1-Cu1-Se2′-C2′	−179.3(2)
Se2-Cu1-Se2′	180	Se2-Cu1-Se1′-C1′	−178.4(2)
Se3-Cu1-Se3′	180	Se3-Cu2-Se4′-C6′	176.8(2)
Se4-Cu1-Se4′	180	Se4-Cu2-Se3′-C5′	−175.5(2)
Se1-Cu1-Se2	93.097(18)	Se1-C1-C2-N2	174.7(4)
Se1-Cu1-Se2′	86.903(18)	Se2-C2-C1-N1	175.1(4)
Se3-Cu1-Se4	92.681(18)	Se3-C5-C6-N4	177.6(4)
Se3-Cu1-Se4′	87.319(18)	Se4-C6-C5-N3	177.9(4)
O1-Li1-N1	108.2(5)	N1-C1-Se1-Cu1	−176.5(4)
O2-Li1-N1	103.1(4)	N2-C2-Se2-Cu1	−176.8(4)
O3-Li1-N1	115.5(5)	N3-C5-Se3-Cu2	−175.7(4)
O2-Li1-O1	112.1(5)	N4-C6-Se4-Cu2	178.3(4)
O3-Li1-O1	113.9(5)		
O3-Li1-O2	103.5(5)		

coordinated only by one N from one $[Cu(pds)_2]^-$ ion and three O atoms from water molecules. Thus, lithium cations have tetrahedral geometry and, differently from the sodium salt **1**, one-dimensional chains are formed by hydrogen bonding (Figure 3). In the Li salt, two O–H···O–H hydrogen bonds (O2–H2b···O1 2.085 Å, $\theta = 169.5°$; O3–H3a···O2 2.074 Å, $\theta = 173.5°$) are present between water molecules coordinated to different Li cations along *a* and between the parallel stacks of $[Cu(pds)_2]^-$ complexes (the Li–Li distance is 4.619 Å; see Figure 2c and Figure 3). Therefore, pds moieties act as bidentate (two Se atoms coordinated to Cu) or tridentate (two Se atoms coordinated to Cu and one N atom coordinated to Li) ligands in the two crystallographically independent complex units.

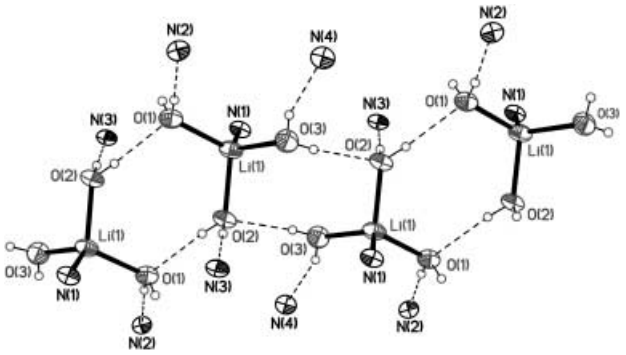

Figure 3. Supramolecular infinite chain formed by the hydrogen-bond network between water molecules coordinated to different Li atoms in **2**. Note the tetrahedral O_3N coordination environment of Li centers.

Moreover, stacks of Li-coordinated $[Cu(pds)_2]^-$ complexes with roughly perpendicular orientation are connected through two different hydrogen bonds. Each $[Cu(pds)_2]^-$ unit exhibits two Se···H–C contacts (Se1···H4–C4 3.015 Å, $\theta = 155°$)[20] between the H atoms of the pds ligand and the closest Se atoms of the perpendicular complexes of the neighboring stacks. At the same time each complex shows two strong N···H–OH hydrogen bonds (N2···H–O 1.948 Å, $\theta = 176°$)[21] between the uncoordinated N atom and the H atom of a water molecule that belongs to the coordination sphere of the Li atom. In the case of Li-uncoordinated $[Cu(pds)_2]^-$ complexes, two Se···H–C contacts (Se3···H8–C8 3.039 Å, $\theta = 150°$) are also observed, and four strong N···H–OH hydrogen bonds (N3···H–O 1.935 Å, $\theta = 179°$; N4···H–O 2.069 Å, $\theta = 159°$) are found between the four uncoordinated N atoms and the H atoms of water molecules. Together all of the above interactions create the 3D framework of the entire structure.

The structure is strongly held together thanks to the coordination of lithium by two N atoms of the same complex unit and multiple hydrogen bonds between Se and aromatic H atoms of the anion and between N and H(water). The stacks of anions are segregated and skewed, and lithium and water molecules form a type of infinite chain that differs from that of the sodium complex **1**[19] (hydrogen-bond network in **2** versus a pure Na–water coordination chain in **1**).

*TBA[$Cu^{III}(pds)_2$] (**3**)*: Complex **3** was characterized as square-planar Cu^{III} complex by NMR spectroscopy and single-crystal X-ray diffraction (see Table 1 for crystal data) on a black block-shaped crystal obtained by recrystallization from diethyl ether/acetonitrile.

The asymmetric unit contains two pds ligands and one TBA cation in general positions, and two half Cu atoms located at symmetry centers. The ORTEP plot of the anion fragment $[Cu^{III}(pds)_2]^-$ (Figure 4) shows a square-planar geometry around the Cu center in the two crystallographically independent complex units, which have very similar bond lengths and angles (see Table 3). All the Cu–Se bond lengths are close to 2.30 Å (see Table 3). However, as shown in Figure 4, a small distortion from planarity of the whole complex is observed in which the rings are twisted in the direction parallel to the long axis of the complex with respect

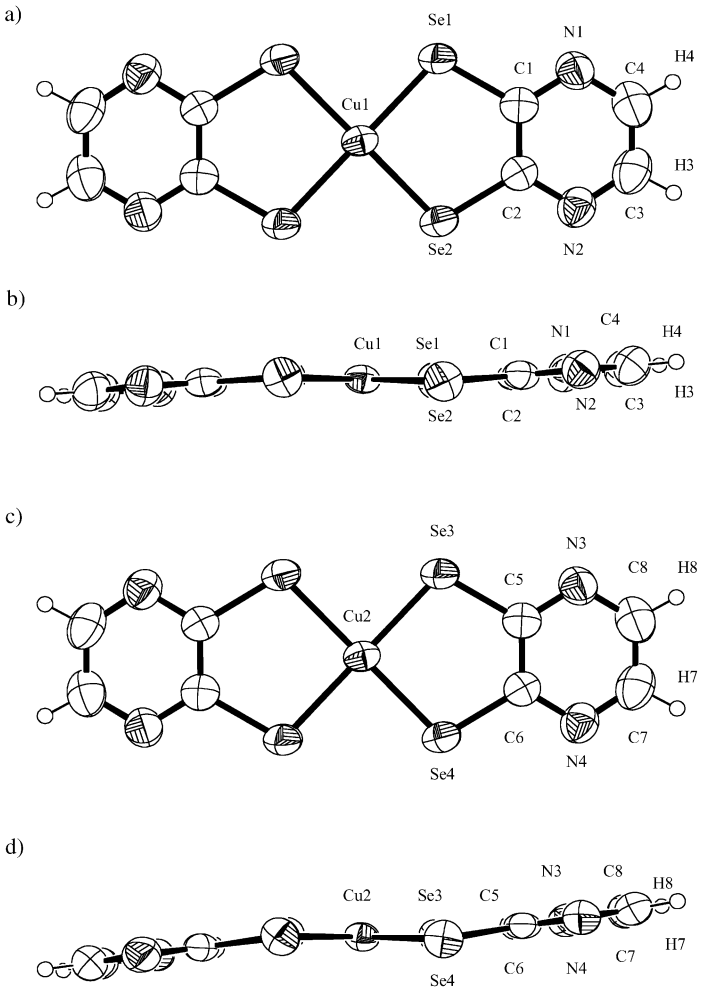

Figure 4. ORTEP plot of the two crystallographically different $[Cu^{III}(pds)_2]^-$ monoanions for complex TBA[$Cu^{III}(pds)_2$] (**3**) in perpendicular (a, c) and parallel (b, d) views to the $CuSe_4$ plane, respectively.

Table 3. Selected bond lengths [Å] and angles [°] for TBA[$Cu^{III}(pds)_2$] (**3**).

Cu1–Se1	2.3065(5)	Cu2–Se3	2.3049(4)
Cu1–Se2	2.3023(4)	Cu2–Se4	2.3010(4)
Se1–C1	1.897(4)	Se3–C5	1.899(4)
Se2–C2	1.888(4)	Se4–C6	1.900(4)
Cu1···Cu2	9.1169(3)		
Se1-Cu1-Se1′	180.0	Se3-Cu2-Se4′-C6′	−171.2(1)
Se2-Cu1-Se2′	180.0	Se4-Cu2-Se3′-C5′	172.0(1)
Se3-Cu1-Se3′	180.0	Se1-C1-C2-N2	177.8(3)
Se4-Cu1-Se4′	180.0	Se2-C2-C1-N1	178.9(3)
Se1-Cu1-Se2	92.971(16)	Se3-C5-C6-N4	179.3(3)
Se1-Cu1-Se2′	87.029(16)	Se4-C6-C5-N3	177.9(3)
Se3-Cu1-Se4	92.309(15)	N1-C1-Se1-Cu1	176.6(3)
Se3-Cu1-Se4′	87.691(15)	N2-C2-Se2-Cu1	−174.4(3)
Se1-Cu1-Se2′-C2′	−174.7(1)	N3-C5-Se3-Cu2	174.8(3)
Se2-Cu1-Se1′-C1′	175.3(1)	N4-C6-Se4-Cu2	−173.1(3)

to the $CuSe_4$ plane, in a chair-conformation motif (torsion angles Se1-Cu1-Se2′-C2′ ca. 175°, Se3-Cu2-Se4′-C6′ ca. 172°).

As shown in Figure 5, the unit cell contains four $[Cu(pds)_2]^-$ units with their long axis roughly perpendicular to each other. There are no close contacts between the monoanions, which are surrounded by TBA cations. Several hydrogen bonds are observed between Se and N atoms of the anions and aliphatic C–H bonds of lateral butyl groups of TBA cations. These anionic complexes form two types of layers: TBA cations alternate between the anionic complexes in one layer (anions with a more evident chair conformation), whereas in the other layer anions are packed in a zig-zag parallel mode with N···N, Se···N, and Se···Se contacts not shorter than 3.776, 4.125, and 5.925 Å, respectively (anions with smaller chair distortion). Short C–H···H–C contacts are also found between butyl groups of adjacent TBA cations.

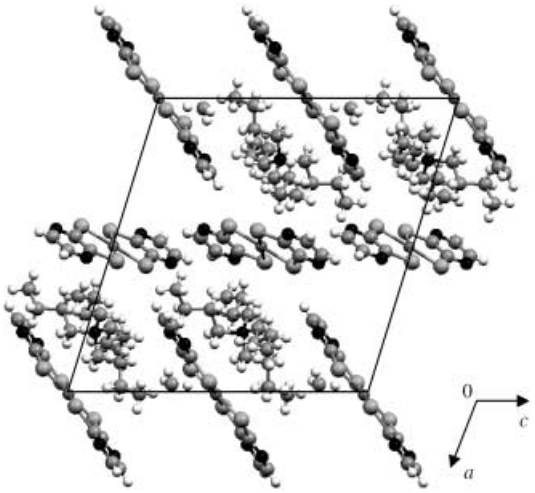

Figure 5. Crystal packing of TBA[$Cu^{III}(pds)_2$] (**3**) in a view along the *b* axis.

*Na[$Cu^{III}(pdt)_2$]·2 H_2O (**4**)*: Complex **4** was characterized as a square-planar Cu^{III} complex by NMR spectroscopy and X-ray diffraction (see Table 1 for crystal data) on a black needle-shaped single crystal obtained by slow diffusion of diethyl ether into a solution of the compound in acetonitrile.

The asymmetric unit contains one pds ligand and one water molecule in general positions, and half Cu and Na atoms at symmetry centers. The ORTEP plot of the anion fragment $[Cu^{III}(pdt)_2]^-$ (Figure 6) shows square-planar geometry around the Cu center, with Cu–S bond lengths close to 2.18 Å. However, as shown in Figure 6b, a small distortion is observed in the planarity of the complex, in which both pyrazine rings are twisted in the same direction with respect to the CuS_4 plane (torsion angle N-C-S-Cu ca. 176°). This deviation from planarity can be explained similarly to that of the selenium analogue **1**, by coordination of the nitrogen atoms of the pyrazine rings to the Na^+ counterion and by the existence of short S···H–C contacts that twist the central and outer parts of the complex in opposite directions. Bond lengths and angles are listed in Table 4.

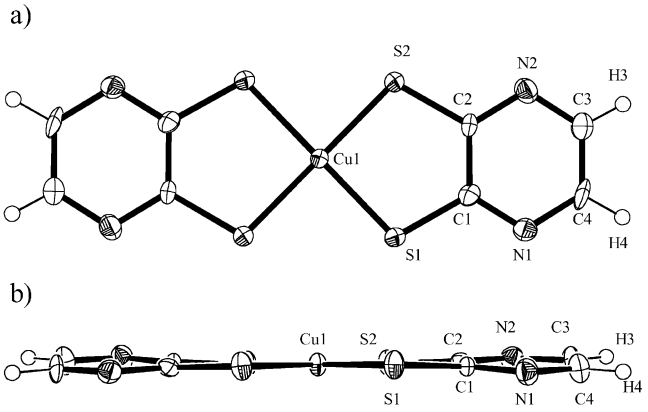

Figure 6. ORTEP plot of the monoanion $[Cu^{III}(pdt)_2]^-$ in Na[$Cu^{III}(pdt)_2$]·2H_2O (**4**) in perpendicular (a) and parallel (b) views to the molecular plane.

As shown in Figure 7, the unit cell contains two $[Cu^{III}(pdt)_2]^-$ units with their long axes almost perpendicular to each other. These anionic complexes form tilted regular stacks along the *a* axis with an average distance between stacked units of 3.45 Å. The angle between the stacking axis *a* and the average $Cu(pdt)_2$ plane is 27°. Lateral offset values of adjacent complexes in the stack of about 1.1 and about 1.5 Å for the long and short axes of the complex, respectively, are also observed (see Figure 7b and c). The crystal packing of **4** is similar to that of the Li salt **2** and almost identical to that of the Na salt **1**.[19]

The sodium ions are coordinated by two nitrogen atoms from two $[Cu^{III}(pdt)_2]^-$ ions with parallel orientation, and four oxygen atoms of water molecules. Thus, one-dimensional chains of alternating Na ions and two water molecules along *a* are formed between the parallel stacks of $[Cu^{III}(pdt)_2]^-$ complexes (Figure 8).

Table 4. Selected bond lengths [Å] and angles [°] for $[Cu^{III}(pdt)_2]\cdot 2H_2O$ (**4**).

Cu1-S1	2.1810(11)	Na1-N1	2.594(4)
Cu1−S2	2.1833(12)	Na1−O1(eq)	2.482(4)
S1−C1	1.742(5)	Na1−O1(ax)	2.651(4)
S2−C2	1.732(5)	Na1···Na1′	3.8400(2)
Cu1···Cu1	3.8400(2)		
S1-Cu1-S2	92.39(4)	N1-Na1-O1(ax)′	91.31(12)
S1-Cu1-S1′	180.0	O1(ax)-Na1-O1(eq)′	81.85(14)
S1-Cu1-S2′	87.61(4)	O1(ax)-Na1-O1(eq)	98.15(13)
S2-Cu1-S2′	180.0	S2-C2-C1-N1	173.6(3)
O1(eq)-Na1-O1(eq)	180.0	S1-C1-C2-N2	174.5(3)
N1-Na1-O1(eq)	92.13(13)	N1-C1-S1-Cu1	−175.2(3)
N1-Na1-O1(eq)′	87.87(13)	N2-C2-S2-Cu1	−177.1(3)
N1-Na1-O1(ax)	88.69(12)		

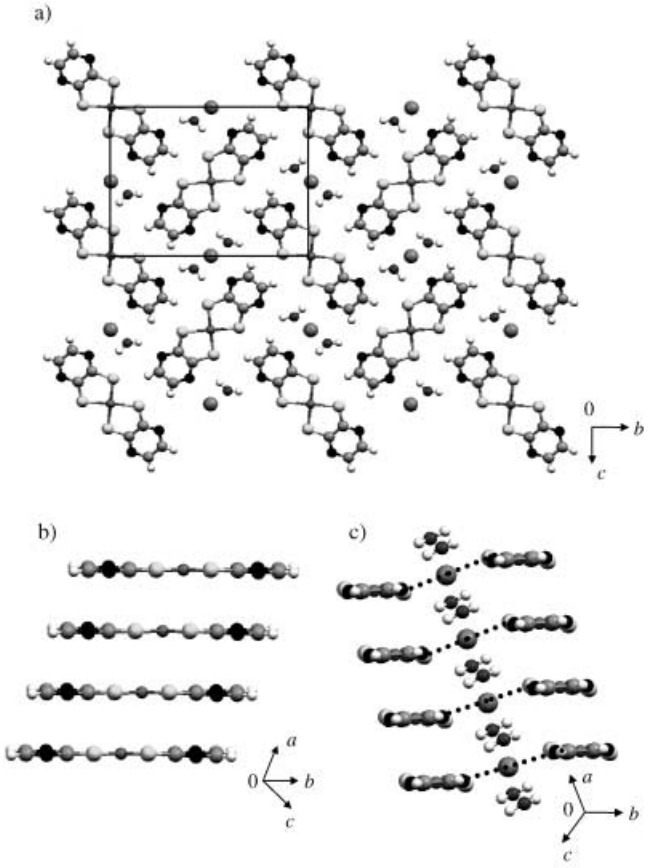

Figure 7. Crystal structure of $Na[Cu^{III}(pdt)_2]\cdot 2H_2O$ (**4**). a) View along the stacking axis *a*. b) Stack of complex units viewed along their shortest axis. c) Parallel stacks of complex units viewed along their longest axis and connected by Na coordination.

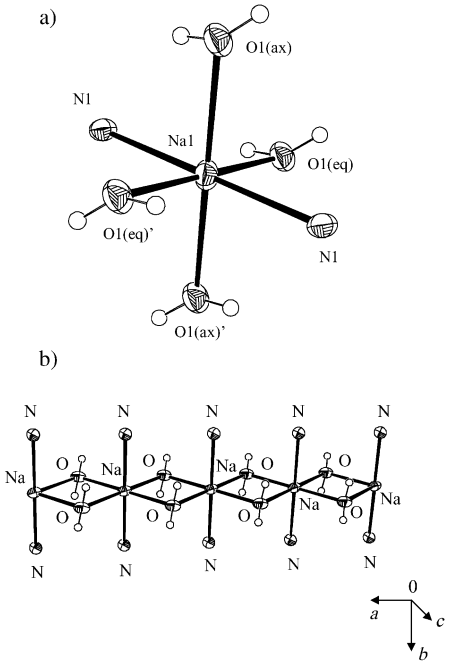

Figure 8. a) Octahedral N_2O_4 coordination environment of Na centers in **4**. b) Infinite chain of -Na-$(\mu$-$O_{aq})_2$-Na-$(\mu$-$O_{aq})_2$- atoms along the molecular stacking axis *a*.

In addition, stacks of $[Cu^{III}(pdt)_2]^-$ complexes with perpendicular orientation are connected through two different hydrogen bonds. Each $[Cu^{III}(pdt)_2]^-$ unit has four short S···H−C contacts (S1···H3−C3 2.873 Å, $\theta = 163°$; S2′···H4−C4 2.985 Å, $\theta = 129°$)[20] between the H atoms of the pdt ligand and the closest S atoms of the perpendicular complexes of the neighboring stacks. At the same time each complex shows two moderately strong N···H−OH hydrogen bonds (N2···H−O 2.142 Å, $\theta = 146°$)[21] between the uncoordinated N atom and the H atom of a water molecule that belongs to the coordination sphere of the Na atom. All these interactions create the 3D framework of the whole structure.

The structure is strongly maintained thanks to the coordination of sodium by two N atoms of different anion moieties, S···H−C contacts, and multiple hydrogen bonds between anion S and aromatic H atoms, N and H(water), S and H(water), and so on. The stacks of anions are segregated, and the sodium and water molecules can be regarded as an infinite ···Na-$(\mu$-$O_{aq})_2$-Na-$(\mu$-$O_{aq})_2$··· chain with an Na−Na distance of 3.8400(2) Å, as depicted in Figures 7c and 8b. Therefore, each pdt moiety acts as a tridentate ligand with two S atoms coordinated to Cu and one N atom coordinated to Na.

*TBA[$Cu^{III}(pdt)_2$] (**5**)*: Complex **5** was characterized as a Cu^{III} complex by NMR spectroscopy and X-ray diffraction (see Table 1 for crystal data) on a black block-shaped single crystal obtained by slow diffusion of diethyl ether into a solution of the compound in acetonitrile.

The asymmetric unit contains one $[Cu^{III}(pdt)_2]^-$ monoanionic complex unit and one TBA cation in general positions. The ORTEP plot of the anion fragment $[Cu^{III}(pdt)_2]^-$ (Figure 9) shows a distorted square-planar geometry around the Cu atom, with crossed S-Cu-S angles close to 170° (see Table 5). All Cu−S bond lengths are close to 2.18 Å (see Table 3). The CuS_4 atoms do not lie in the same plane as shown in Figure 9, and the two pds moieties are twisted with an average angle of 5° (see Table 5).

As shown in Figure 10, the unit cell contains four $[Cu^{III}(pdt)_2]^-$ units with their long axes roughly perpendicular to each other. The monoanions are almost surrounded

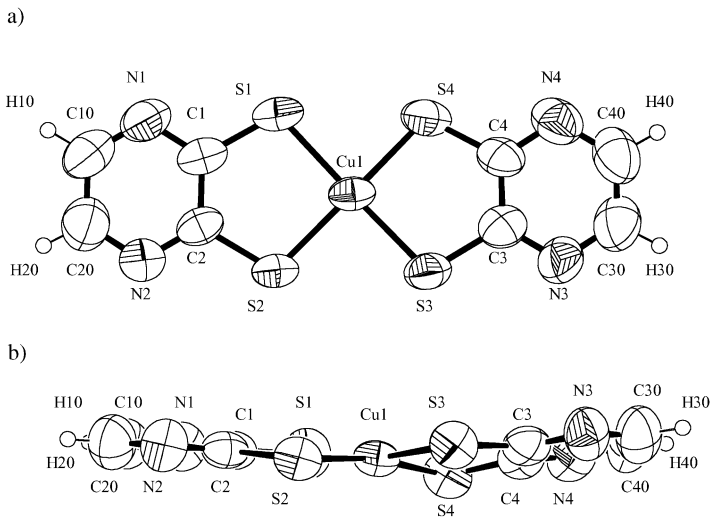

Figure 9. ORTEP plot of the monoanion $[Cu^{III}(pdt)_2]^-$ in $[Cu^{III}(pdt)_2]$-TBA (**5**) in perpendicular (a) and parallel (b) views to the molecular plane.

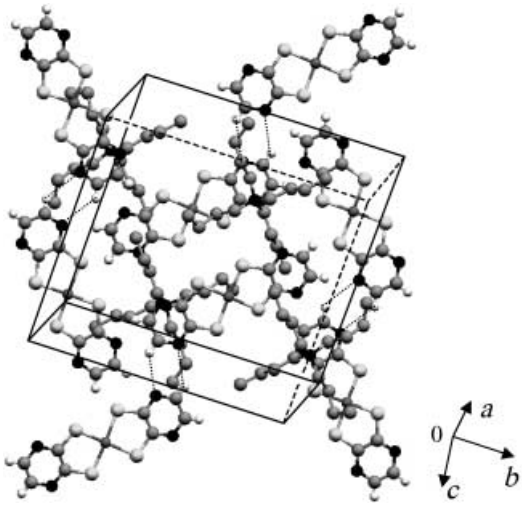

Figure 10. Crystal packing of complex $[Cu^{III}(pdt)_2]$TBA (**5**) in a perpendicular view to the molecular plane. H atoms of TBA are omitted for clarity.

Table 5. Selected bond lengths [Å] and angles [°] for $[Cu^{III}(pdt)_2]$TBA (**5**).

Cu1–S1	2.1751(18)	Cu1–S3	2.1749(18)
Cu1–S2	2.179(2)	Cu1–S4	2.179(2)
S1–C1	1.726(7)	S3–C3	1.733(7)
S2–C2	1.747(6)	S4–C4	1.724(7)
Cu1···Cu1′	8.313 (7)		
S1-Cu1-S2	92.61(7)	S4-Cu1-S1-C1	172.0(2)
S1-Cu1-S3	170.23(8)	S1-C1-C2-N2	178.2(2)
S1-Cu1-S4	87.40(8)	S2-C2-C1-N1	177.6(2)
S2-Cu1-S3	88.94(7)	S3-C3-C4-N4	177.9(2)
S2-Cu1-S4	170.27(7)	S4-C4-C3-N3	177.5(2)
S3-Cu1-S4	92.70(7)	N1-C1-S1-Cu1	179.4(2)
S1-Cu1-S4-C4	161.9(2)	N2-C2-S2-Cu1	−177.2(2)
S2-Cu1-S3-C3	177.6(2)	N3-C3-S3-Cu1	175.5(2)
S3-Cu1-S2-C2	167.1(2)	N4-C4-S4-Cu1	−172.6(2)

by tetrabutylammonium cations but, distinct from TBA-$[Cu^{III}(pds)_2]$ (**3**), two important N1···H10–C10 hydrogen bonds (2.740 Å, 134.0°) are found, resulting in the formation of pairs of staggered parallel anions (Figure 10). In this case several hydrogen bonds are also observed between S and N atoms of the anions and aliphatic C–H bonds of lateral butyl groups of TBA cations. The pairs of parallel anion complexes alternate with other pairs in a perpendicular packing motif. However, the closest Cu···Cu distance is 8.313 Å due to the intermediate TBA cations (along the *c* axis). Short C–H···H–C contacts are also found between butyl groups of adjacent TBA cations.

Discussion

Structural comparison: The crystal structure of $Na[Cu^{III}(pds)_2]\cdot 2H_2O$ (**1**)[19] showed that the N atoms of the aromatic rings of the pds ligand are in fact open coordination positions that become crucial in the construction of the crystal packing. Therefore, we used two strategies to explore this phenomenon: first, we decided to synthesize the same complexes but with different counterions, either another alkali metal cation or bulky, noncoordinating cations such as TBA^+. We also considered reducing the global volume of the complex, and hence attempted synthesize more compact structures by using the S-containing pdt ligand.

Comparison of the structures allows the influence of the bulkiness of the chalcogen atoms on the 3D crystal structure to be studied. It can be concluded that $Na[Cu^{III}(pdt)_2]\cdot 2H_2O$ (**4**) has the most compact structure, in which intermolecular distances are shorter (3.45 Å), as is the Na···Na distance (3.840(5) Å). In the selenium analogue $Na[Cu^{III}(pds)_2]\cdot 2H_2O$ (**1**) both the intermolecular distances (3.56 Å) and the Na···Na distance (4.0446(2) Å) are larger,[19] in agreement with the bulkiness of Se compared to S. Indeed, the compactness of the structure of **4** is not only reflected in the shorter intermolecular distances but also in the one-dimensional ···Na-(μ-O_{aq})$_2$-Na-(μ-O_{aq})$_2$··· chains, and specifically in the distortion of the octahedral geometry around the alkali metal ion. Thus, axially distorted Na–O_{ax} bond lengths are 2.97 Å for **1**, but only 2.65 Å for **4** due to the compact structure of the latter salt. The unit cell parameters also reflect the same behavior, being slightly smaller for **4** (see Table 1).

In contrast, with the selenium ligand analogue and lithium as counterion, that is, $Li[Cu^{III}(pds)_2]\cdot 3H_2O$ (**2**), the smaller size of lithium compared to sodium sterically precludes the formation of one-dimensional ···Li-(μ-O_{aq})$_2$-Li-(μ-O_{aq})$_2$··· chains similar to those formed with sodium.[19] Furthermore, the smaller atomic size of lithium favors a tetrahedral instead of a octahedral geometry around the alkali metal cation. Nevertheless, an Li–H_2O network, mediated by hydrogen bonds also forms a one-dimensional supramolecular chain that stabilizes the structure, in a similar manner to **1** and **4**.

The use of alkali metal ions in the synthesis of complexes with potential coordination positions (e.g., aromatic N) in the ligand backbone completely modifies the 3D framework

of the crystal. This fact is highlighted if we compare the structures of the TBA salts with those of the alkali metal salts with either the selenium or sulfur ligands. In TBA-$[Cu^{III}(pds)_2]$ (**3**), the monoanionic complexes are isolated by the bulky TBA^+ cations, and no short contacts or hydrogen bonds are detected between the anions. Similarly, the crystal structure of $[Cu^{III}(pdt)_2]$TBA (**5**) also does not exhibit segregated stacks of anions. Instead, and in contrast to the Se analogue **3**, hydrogen-bonded stabilized pairs of $[Cu^{III}(pdt)_2]^-$ ions are present, thanks to two interactions between N and C–H of the aromatic ring.

Copper(III) generally exhibits square-planar geometry,[22a] although square-pyramidal[23] and octahedral geometries have also been reported.[24] The coordination geometry for Cu in complexes **1** and **2** is mainly square-planar but two Se atoms also interact weakly (Cu···Se ~3.5–3.6 Å) in an axial positions along the stacking axis. Therefore, an axially elongated octahedral geometry could also be envisioned for this system. A similar situation is found in complex **4**, with an axial Cu···S interaction of 3.46 Å. Complexes **3** and **5** have square-planar and distorted square-planar geometry around Cu, respectively.

Electronic structure: The metal bis-1,2-diselenolene complexes reported here resemble the square-planar, diamagnetic transition metal complexes containing two bidentate ligands derived from *o*-catecholates,[8] *o*-phenylenediamines,[9] *o*-benzodithiolates,[10,11] *o*-aminophenolates,[12–15] *o*-aminothiophenolates[16] and *o*-amidochalcogenophenolates.[17] Therefore, the characterization of the electronic structure is a key issue, and the question of describing the diselenolene ligand as an innocent or noninnocent ligand has to be addressed.[12] Wieghardt et al. support the idea that structural and spectroscopic criteria are suitable for establishing the oxidation state of the metal ions and ligands, and they have devoted much effort to the characterization of the semiquinonate-type ligands in these systems, from cationic to anionic species, and especially the so-called diradical character for neutral species (see Scheme 1).

In general, the open-shell semiquinonate type ligands (Scheme 2) display a typical pattern of three alternating short–long–short C–C bond lengths, whereas in closed-shell aromatic ligands, which may be present in dianionic, monoanionic, or neutral species, the six C–C bonds of the phenyl entity are equivalent. In compounds **1**–**5** studied here, well-resolved crystal structures do not indicate a short–long–short pattern for pds or pdt ligands (see Table S1 in the Supporting Information). Another important structural feature usually observed is shortening of the C–X bond (X = O, N, S) by about 0.04 Å which indicates formation of the monoanionic π-radical *o*-semiquinonato species.[25] In selenium-containing complexes **1**–**3**, the average C–Se distance is 1.89 Å, which is 0.01 Å longer than in *trans*-$[Ni(-SeC_6H_4-o-NH-)_2]^-$, which was characterized as a delocalized *o*-amidoselenophenolate(2–)/*o*-iminoselenobenzosemiquinonate(1–) π radical.[17] In sulfur-containing complexes **4** and **5**, the average C–S distance is 1.74 Å, which is again 0.01 Å longer than that observed in the delocalized phenolate/semiquinonate complex *trans*-$[Ni(-SC_6H_4-o-NH-)_2]^-$, and 0.02 Å longer than in N,S-coordinated *trans*-$[Ni(L^{ISQ})_2]$, characterized as a bis[*o*-iminothiobenzosemiquinonate(1–)] π radical complex. The structural description of our systems resembles much more closely that of $[Fe(bdt)_2(PMe_3)]$,[26] in which the bdt^{2-} (1,2-benzenedithiolate) ligand was characterized as an innocent ligand, and it was concluded that oxidative processes occur on the FeS_4 unit and do not extend to the aromatic moieties.

X-ray crystallography is again a good method to deduce the oxidation state of the metal by focusing on the Cu–Se and Cu–S bond lengths, as they are shorter for higher oxidation states. The Cu–Se bond lengths in **1**–**3** are roughly 2.30 Å, about 0.11 Å shorter than Cu–Se bond lengths in Cu^{II} selenium coronands.[27] In complexes **4** and **5**, the Cu–S bond lengths are 2.18 Å, about 0.10 Å shorter than those of other Cu^{II} bis-dithiolene complexes.[22a,28] The latter structural changes also argue in favor of an important contribution of the metal to the oxidative processes of complexes **1**–**5**.

Cyclic voltammetry on compounds containing bidentate *ortho*-disubstituted aromatic ligands usually show a rich electrochemistry for neutral species owing to the noninnocence of the ligands, since all undergo two successive one-electron oxidations and reductions that make the mono- and dications and the mono- and dianions accessible species.[7] This electrochemical behavior is clearly not displayed by complexes **1**–**5,** and only one reversible Cu^{II}/Cu^{III} wave is found at $E_{1/2} = -0.54$ and -0.33 V for Se-containing complexes **1**–**3** and S-containing **4** and **5**, respectively (Figure 11). These very low potentials indicate a notable destabilization of dianions $[Cu(pds)_2]^{2-}$ and $[Cu(pdt)_2]^{2-}$. On the other hand, only irreversible oxidation processes occur above 1 V, and therefore the stability of a neutral complex is electrochemically not favored. Furthermore, the sensitivity of the redox potentials on changing the transition metal to Ni^{III} is further evidence that these complexes are at least not exclusively ligand centered.[29]

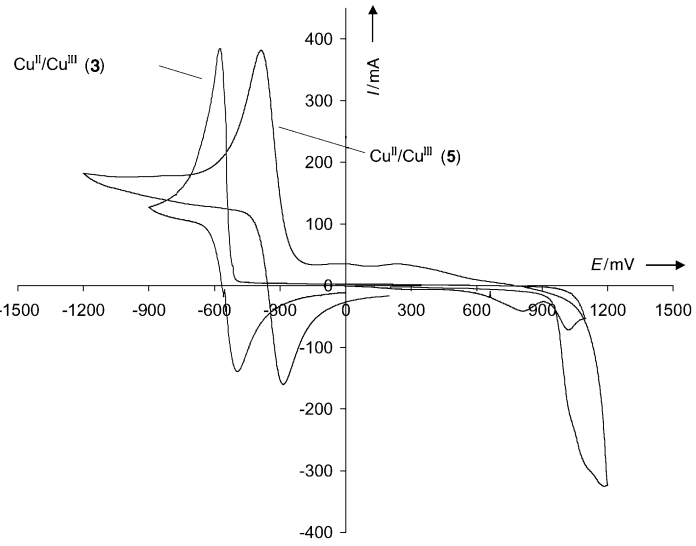

Figure 11. Cyclic voltammograms of **3** and **5** in CH_3CN showing quasireversible waves at $E_{1/2} = -0.54$ and -0.33 V versus Ag/AgCl (scan rate: 100 mV s^{-1}; 0.1 M $TBAPF_6$ as supporting electrolyte).

The electronic spectra of all complexes are also in accordance with an innocent character of the ligands. For noninnocent ligands, it has been reported that the electronic spectra of neutral complexes, dications, dianions, monocations, and monoanions are characteristic of the oxidation state of the two ligands irrespective of the nature of the central metal ion (Ni^{II}, Pd^{II}, Pt^{II}) or the substitution pattern of the *o*-aminophenolate or *o*-aminothiophenolate ligands.[7] All these species show relatively intense π–π* transitions of the respective ligand in the 300–1100 nm range. The $[M^{II}(L^{ISQ})(L^{AP}\text{-}H)]^-$ monoanions exhibit a very intense absorption at wavelengths longer than 900 nm with $\varepsilon \approx 10^4\ cm^{-1}M^{-1}$,[16] whereas the monoanionic $[Cu^{III}(pds)_2]^-$ complexes **1**–**3** have much weaker low-energy bands at 596 nm ($\varepsilon = 950\ cm^{-1}M^{-1}$) and 921 nm ($113\ cm^{-1}M^{-1}$), while a intense band appears at 386 nm ($4\times10^4\ cm^{-1}M^{-1}$). We observe a shift in the low-energy bands for $[Cu^{III}(pdt)_2]^-$ complexes **4** and **5** to 536 nm ($650\ cm^{-1}M^{-1}$), 1012 nm ($195\ cm^{-1}M^{-1}$), and a similar band at 379 nm ($5\times10^4\ cm^{-1}M^{-1}$; see Figure 12). The higher

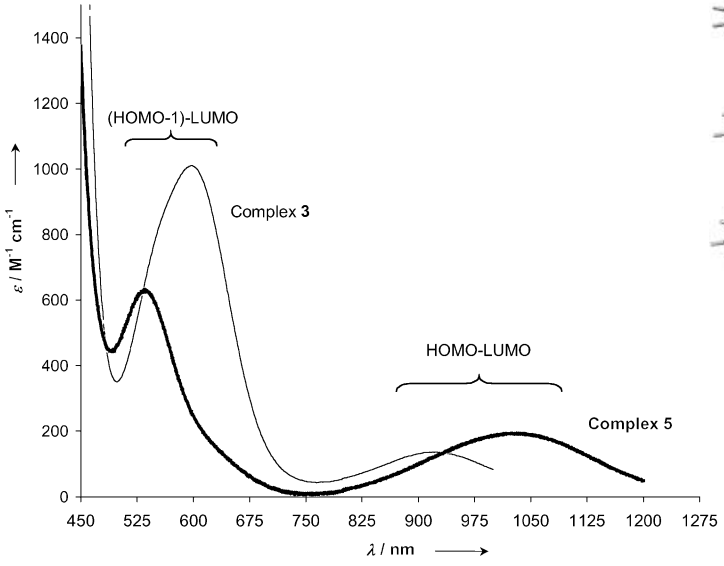

Figure 12. Electronic spectra of **3** (thin line) and **5** (thick line) in CH_3CN, and assignment of the bands (see text).

energy band at 380 nm is also observed in the electronic spectra of the pds^{2-} and pdt^{2-} disodium salts, but it is an order of magnitude weaker ($\varepsilon \approx 6\times10^3\ cm^{-1}M^{-1}$) than in the complexes. The peaks in the visible region of the electronic spectra are specifically assigned to a (HOMO-2)–LUMO transition for the band centered at 380 nm, (HOMO-1)–LUMO transition for the band at 596 and 536 nm for $[Cu^{III}(pds)_2]^-$ and $[Cu^{III}(pdt)_2]^-$, respectively, and HOMO–LUMO transitions for the lower energy bands at wavelengths values higher than 900 nm. The shifts observed between the Se- and S-containing complexes are attributed to differences in the energy levels of the respective frontier orbitals, which are mainly delocalized over the $CuSe_4$ and CuS_4 units (see ab initio calculations below). This assignment was confirmed by TDDFT calculations including solvent effects with a CPCM model (see Experimental Section). The values obtained for the vertical excitations for $[Cu(pds)_2]^-$ and $[Cu(pdt)_2]^-$ are 654, 678, and 1129 nm, and for $[Cu(pdt)_2]^-$ 608, 707, and 1292 nm. Although the magnitude of the excitation is well reproduced, there is a clear overestimation in comparison with experimental data. This is probably due to the anionic nature of the molecules.

Density functional calculations were performed on $[Cu(pds)_2]^-$ and $[Cu(pdt)_2]^-$ in order to understand the electronic structure of such compounds. The frontier orbitals were calculated and their structures optimized (see Methods of Calculation in Experimental Section). The calculated bond lengths and angles for $[Cu(pds)_2]^-$ completely agree with the experimental ones obtained by X-ray diffraction (Table S2 and S3, Supporting Information). Thus, the frontier orbitals depicted in Figure 13 can be described as follows. For both molecules, the orbital composition is almost the same, the main difference being the opposite relative stabilities of the HOMO-1 and HOMO-2 orbitals. The HOMO is an out-of-plane π orbital mainly consisting of a combination of the p_z chalcogen orbitals with a small contribution from the Cu d orbitals. The two electrons are therefore mainly delocalized on the Se atoms.

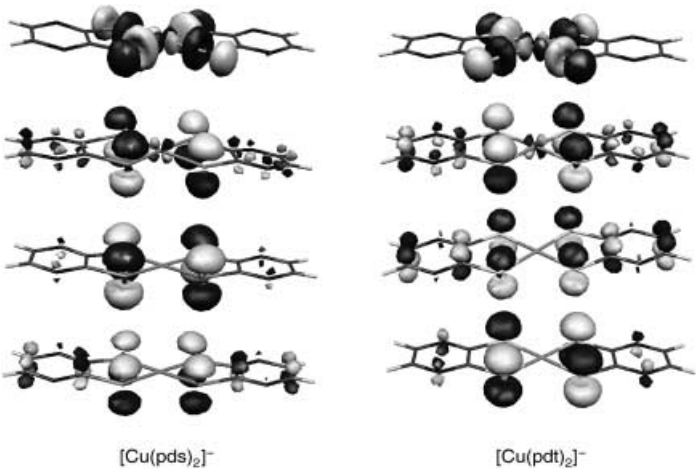

Figure 13. Frontier MOs of the $[Cu(pds)_2]^-$ and $[Cu(pdt)_2]^-$ monoanions obtained from B3LYP calculations (from LUMO to HOMO-2). The orbitals are ordered by energy with the LUMO placed above.

The LUMO is the σ antibonding combination of the Cu d_{xy} and the chalcogen p_x and p_y orbitals with a large contribution from Cu. This character is clearly reflected in a considerable increase (by around 0.12 Å) of the Cu–Se bond length for $[Cu(pds)_2]^{2-}$ (see Table S2 in the Supporting Information). These contributions rule out the possibility of considerable mixing of p_z with Cu d_{xz} and d_{yz} orbitals through a M–L π bond, which would explain the delocalized oxidation state of the metal and ligands in an $L\text{-}M^{II}\text{-}L^{*}\leftrightarrow L\text{-}M^{III}\text{-}L$ equilibrium, as was proposed for *trans*-$[Ni(SeC_6H_4\text{-}o\text{-}NH)_2]^-$.[17] Furthermore, the frontier orbitals calculated for $[Cu(pds)_2]^-$ are similar to those reported by Solomon et al. for $[Ni(S_2C_2Me_2)_2]^-$,[30] although in complexes **1**–**5** no contribution of the C=C moiety bound to the chalcogen atoms is found in the HOMO. From the LUMO of the

$[Ni(S_2C_2Me_2)_2]^-$ complex, extensive charge donation from the σ ligand orbitals to the Ni atom is deduced. The removal of electron density from the σ antibonding orbitals of the dithiolene ligands results in a net bonding interaction between them and consequently in short inter- and intraligand S···S distances (intra 3.08 Å, inter 3.02 Å). These short Se···Se and S···S distances are also observed in complexes **1**–**5**, respectively, in line with the DFT calculations and with the general electronic description of these systems (see Table S1 in the Supporting Information). The conclusion that was reached by Solomon et al.,[30] also supported by XAS experiments, indicates the presence of limited spin polarization on the dithiolene ligands, that is, diradical character of the complex. One condition that must be fulfilled for the diradical character of these systems is that a broken-symmetry solution must occur when mixing the HOMO and LUMO orbitals.[25] If we analyze the nature of the frontier orbitals, a possible diradical character should be expected for $[Cu(pdt)_2]$. In this case, the mixture of the HOMO and HOMO-1 orbitals (see Figure 13) can generate an instability in the wavefunction to give a broken-symmetry solution with diradical character, but that would only happen in the monocationic system, which is not even detected in the cyclic voltammogram. In the case of $[Cu(pds)_2]$ such instability can be obtained by mixing the HOMO and HOMO-2, which could be expected to be more difficult. Similarly, Wieghardt et al. came to a similar conclusion for the Ni complexes of *o*-dithiosemiquinolato-type ligands, for which it is indeed observed that the diradical character decreases in the order of O > N > S donors.[25] This sequence can be understood in terms of the stability of the semiquinone forms of the ligands, which depends on the ability of the coordinating atom to form partial double bonds with the ring carbon atoms. This ability increases in the series S < N < O.[25,31]

The theoretically calculated bond lengths and angles for the DFT-optimized structure of the hypothetical neutral species $[Cu(pds)_2]$ does not show any remarkable structural difference (see Table S2 in the Supporting Information) compared to the monoanion $[Cu(pds)_2]^-$. This fact can be understood in terms of the nonbonding Se–Cu character of the HOMO, which can be considered as an indication that the oxidation is mainly supported by the Se atoms with no participation of the aromatic ring. As mentioned, the neutral species have not been obtained experimentally due to their instability (see above).

In summary, the not physically detected diradical character of bis-diselenolene complexes **1**–**3** and bis-dithiolene complexes **4** and **5** agrees with the theoretical analysis of the calculated frontier orbitals. Due to the nature of the orbitals a possible diradical character should be expected for $[Cu(pdt)_2]$, but is experimentally discounted, as well as for $[Cu(pds)_2]$. From the experimental and theoretical point of view, we may conclude that Se donor atoms are similarly or less capable than S atoms of forming partial double bonds, and the seriously diminished ability to act as *o*-semiquinolato type ligands favors stabilization of the aromatiticy of the pyrazine ring.

We can also conclude that oxidation state Cu^{II} is destabilized with respect to Cu^{III}. A d^8 electronic configuration of a transition-metal complex favors an square-planar geometry, as is observed in complexes **1**–**5**. The important metal contribution to the frontier orbitals was not observed in other bis-dithiolene complexes described in the literature some years ago, in which the redox process is considered to be exclusively ligand-centered on the basis of Raman spectroscopic results.[6] The question of metal- or ligand-centered redox processes in bis-dithiolene complexes was also investigated by using X-ray photoelectron spectroscopy as a direct method to evaluate the binding energies E_b of the electrons on the central metal atom and on the ligand atoms, but with inconclusive results.[32] More recent studies have overcome these ambiguities by a combination of different experimental techniques and ab initio calculations. At this point, an unequivocal technique such as X-ray absorption spectroscopy (XAS) emerges as a definitive proof of the true oxidation states of the metal and the ligands.[30,33] Copper, selenium, and sulfur K-edge XAS experiments on complexes **1**–**5** are currently in progress, and results will be published elsewhere.

Electrical conductivity measurements on single crystals of complexes **1**, **2**, and **4** revealed insulating behavior despite the presence of well-defined segregated stacks that can favor the formation of electronic bands. This is an expected behavior for nonmixed-valence (closed-shell, d^8) complexes with strongly localized charges, since the redox potential of the complexes has been found to be inappropriate for obtaining conducting mixed-valence Cu^{II}/Cu^{III} compounds. Nevertheless, their use as building blocks in the synthesis of radical ion salts or charge-transfer compounds[34] is promising and will be reported elsewhere.

Conclusions

Complexes **1**–**3** are the first structurally characterized Cu^{III} compounds with an Se_4 coordination environment for the central metal atom.[19,22a] The sulfur analogues **4** and **5** were synthesized to evaluate the electronic influence of the nature of coordinating atoms (Se versus S) on the stabilization of the high oxidation state Cu^{III} and the structural influence on the crystal-engineering possibilities due to the different atomic size of the chalcogen atom. Although the oxidation state of +3 for copper is still considered rare, a growing number of crystal structures of Cu^{III} complexes has been reported.[22] The proven stability of the +3 oxidation state for Cu in adequate ligand environments is in line with all the experimental and theoretical data on complexes **1**–**5**, and leads us to conclude the non-existence of a π-radical *o*-semiquinolato-type ligand in both selenium- and sulfur-containing systems, so that both ligands can be considered to be innocent.

In the context of synthetic metals, the preparation of Cu^{III} complexes such as $Na[Cu^{III}(pds)_2]\cdot 2H_2O$ (**1**),[19] $Li[Cu^{III}(pds)_2]\cdot 3H_2O$ (**2**), and $Na[Cu^{III}(pdt)_2]\cdot 2H_2O$ (**4**), which form well-ordered stacks of complex units, opens the possibility of obtaining molecular metals, provided a mixed-valence situation can be achieved. The present results demonstrate the possibility for crystal engineering of such compounds by co-

ordination of alkali metal counterions with the ring nitrogen atoms of the dithiolene or diselenolene transition-metal complexes. The different size and coordination properties of alkali metal ions permit fine tuning of the 3D crystal structure in these complexes, a situation that may be extrapolated to other systems in a preconceived manner.

Experimental Sections

Materials: Reagent-grade solvents, supplied by SDS, were dried before use by standard methods and stored under argon. Reagents were obtained commercially from Aldrich and used without further purification.

Elemental analyses were performed by SA-UAB (Servei d'Anàlisi-Universitat Autònoma de Barcelona). UV/Vis/NIR spectra were recorded on a Varian Cary 5 spectrophotometer. NMR spectra were recorded on a Bruker DPX 300 MHz spectrometer. Proton chemical shifts were referenced to TMS. IR spectra were obtained on a Perkin Elmer Spectrum One spectrophotometer by using KBr pellets. Cyclic voltammetry were carried out at room temperature with an EG&G (PAR263A) potentiostat/galvanostat in a standard three-electrode cell (Ag/Ag^+ reference) with Pt wire working and auxiliary electrodes. Distilled and argon-degassed acetone or acetonitrile was used as solvent with 0.1 M $TBA^+PF_6^-$ as supporting electrolyte (scan rate: 100 $mV s^{-1}$).

The electrical resistivity was measured along the long axis of selected single crystals by using a four-in-line contact configuration.

Pyrazine-2,3-diselenol (pds) was synthesized by the method described in the literature.[18] Pyrazine-2,3-dithiol (pdt) was prepared by a modification of the literature procedure for pds (see below). $Na[Cu^{III}(pds)_2]\cdot 2H_2O$ (**1**) was prepared according to previously reported procedures.[19]

Caution: Perchlorate salts are potentially explosive and should be handled with care.

Pyrazine-2,3-dithiol (pdt): 2,3-Dichloropyrazine (4.96 g, 33.3 mmol) and NaHS (2.21 g, 39.4 mmol) were refluxed in H_2O (30 mL) with strong stirring under argon for 2 h. The abundant yellow precipitate obtained was filtered off and washed with H_2O. The solid was suspended in H_2O and dissolved by addition of a concentrated aqueous solution of NaOH to pH > 10. The solution was then washed with CH_2Cl_2 (3 × 20 mL) and the aqueous phase was filtered and acidified with glacial acetic acid to pH < 3. The yellow precipitate formed was filtered off, washed with water and acetone, and dried in vacuo to give pure pdt (1.42 g, 30% yield). IR (KBr pellet): $\tilde{\nu}$ = 3133, 3089, 2902, 2780, 1586, 1538, 1392, 1249, 1145, 1039, 785, 645, 499 cm^{-1}; elemental analysis (%) calcd for $C_4N_2S_2H_4$ (144.2): C 33.32, H 2.80, N 19.43, S 44.46; found: C 33.25, H 2.42, N 19.05, S 44.29.

$Na[Cu^{III}(pds)_2]\cdot 2H_2O$ (1): Synthesis as published.[19] Important data for comparison: UV/Vis (CH_3CN): λ_{max}/nm (ε/$cm^{-1}M^{-1}$) = 386 (51 500), 596 (890), 921 (105); CV (in CH_3CN, vs Ag/AgCl): $E_{1/2}$ = −0.54 V.

$Li[Cu^{III}(pds)_2]\cdot 3H_2O$ (2): A solution of LiOH in water (2 M, 0.32 mL, 0.63 mmol) was injected into a suspension of pyrazine-2,3-diselenol (50 mg, 0.21 mmol) in CH_3OH (2.5 mL) magnetically stirred under an argon atmosphere. The reaction mixture changed color from orange to yellow, and the suspended solid dissolved completely. After an additional 5 min of stirring, solid $Cu(ClO_4)_2\cdot 6H_2O$ (38.9 mg, 0.105 mmol) was added, and an air flow was introduced into the flask for 5 min. The solution turned dark green, and after 4 h of strong stirring, the solution was filtered through Celite. Diffusion of diethyl ether into the filered solution yielded pure **2** as dark green crystals (54% yield, 33.5 mg, 0.058 mmol). UV/Vis (CH_3CN): λ_{max} (ε) = 386 (39 400), 596 (950), 921 nm (113 $cm^{-1}M^{-1}$); IR (KBr pellet): $\tilde{\nu}$ = 2962, 1545, 1467, 1417, 1325, 1190, 1142, 1053, 840, 823, 698 cm^{-1}; ^1H NMR (300 MHz, CD_3CN, 25 °C): δ = 8.16 ppm (s, 4H); ^{13}C NMR (300 MHz, CD_3CN, 25 °C): δ = 162.3, 138.2 ppm; elemental analysis (%) calcd for $C_8H_{10}CuN_4LiO_3Se_4$ (596.5): C 16.61, H 1.39, N 9.68; found: C 16.40, H 1.44, N 9.52; CV (in CH_3CN): $E_{1/2}$ (vs Ag/AgCl) = −0.52 V.

$TBA[Cu^{III}(pds)_2]$ (3): An excess of TBABr (60 mg, 0.186 mmol) was added to a solution of **1** (50 mg, 0.084 mmol) in CH_3CN, and the reaction mixture was stirred for 2 h. Exposure of the filtered solution to diethyl ether yielded complex **3** as black crystals (76%, 49.7 mg, 0.064 mmol). UV/Vis (CH_3CN): λ_{max} (ε) = 386 (41 700), 596 (1010), 921 nm (140 $cm^{-1}M^{-1}$); IR (KBr pellet): $\tilde{\nu}$ = 3054, 2955, 2869, 1528, 1483, 1461, 1379, 1320, 1173, 1131, 1040, 842, 737 cm^{-1}; ^1H NMR (300 MHz, CD_3CN, 25 °C): δ = 8.16 (s, 4H), 3.10 (t, 8H), 1.60 (m, 8H), 1.38 (m, 8H), 0.98 ppm (t, 12H); ^{13}C NMR (300 MHz, CD_3CN, 25 °C): δ = 162.2, 138.2, 58.2, 23.1, 19.1, 12.5 ppm; elemental analysis (%) calcd for $C_{24}H_{40}CuN_5Se_4$ (778.0): C 37.05, H 5.18, N 9.00; found: C 37.40, H 5.44, N 8.78; CV (in CH_3CN, vs Ag/AgCl): $E_{1/2}$ = −0.54 V.

$Na[Cu^{III}(pdt)_2]\cdot 2H_2O$ (4): A solution of NaOH in water (2 M, 0.52 mL, 0.70 mmol) was injected into a suspension of pyrazine-2,3-dithiol (50 mg; 0.35 mmol) in CH_3CN (3 mL) with stirring under argon. The reaction mixture changed color to from yellow to pale yellow, and the suspended solid dissolved. After 5 min of stirring, solid $Cu(ClO_4)_2\cdot 6H_2O$ (64.3 mg, 0.18 mmol) was added, and the formed red-brown solution was stirred for 15 min, after which resublimated I_2 (11 mg, 0.087 mmol) was added. After 10 min of strong stirring, the solvent of the brown solution was evaporated and the solid residue redissolved in methanol (3 mL). A green solid appeared in suspension after 1 h of stirring. The solid was collected by filtration and dissolved in acetone to give a brown-red solution, which was filtered through Celite. Slow diffusion of diethyl ether into the acetone solution afforded black needle-shaped crystals of the **4** (62%, 43 mg, 0.11 mmol). UV/Vis (acetone): λ_{max} (ε) = 379 (51 190), 536 (650), 1012 nm (195 $cm^{-1}M^{-1}$); IR (KBr pellet): $\tilde{\nu}$ = 3459, 2963, 2875, 1667, 1546, 1467, 1420, 1337, 1318, 1204, 1150, 1076, 833, 661, 485, 446 cm^{-1}; ^1H NMR (300 MHz, CD_3CN, 25 °C): δ = 8.13 ppm (s; 4H); ^{13}C NMR (300 MHz, CD_3CN, 25 °C): δ = 161.1, 137.0 ppm; elemental analysis (%) calcd for $C_8H_8CuN_4NaO_2S_4$ (406.95): C 23.61, H 1.98, N 13.77, S 31.51; found: C 23.70, H 1.63, N 12.85, S 30.14; CV (in CH_3CN, vs Ag/AgCl): $E_{1/2}$ = −0.30 V.

$TBA[Cu^{III}(pdt)_2]$ (5): Complex **4** (20 mg, 0.049 mmol) was dissolved in acetone (3 mL) and TBABr (40 mg, 0.124 mmol) was added. The solution was stirred overnight, dried with anhydrous $MgSO_4$, and filtered through Celite. Slow diffusion of diethyl ether into this solution yielded prismatic dark red crystals of complex **5** (89%, 25.8 mg, 0.044 mmol). UV/Vis (CH_3CN): λ_{max} (ε) = 379 (47 300), 536 (630), 1020 nm (195 $cm^{-1}M^{-1}$); IR (KBr pellet): $\tilde{\nu}$ = 3079, 2957, 2929, 2870, 1483, 1461, 1417, 1381, 1329, 1190, 1142, 1061, 845, 830, 737, 442 cm^{-1}; ^1H NMR (300 MHz, CD_3CN, 25 °C): δ = 8.13 (s, 4H), 3.11 (m, 8H), 1.63 (q, 8H), 1.38 (q, 8H), 0.98 ppm (t, 12H); ^{13}C NMR (300 MHz, CD_3CN, 25 °C): δ = 167.0, 137.1, 57.9, 23.1, 19.1, 12.5 ppm; elemental analysis (%) calcd for $C_{24}H_{40}CuN_5S_4$ (590.4): C 48.83, H 6.83, N 11.86, S 21.72; found: C 48.60, H 6.82, N 11.55, S 21.40; CV (in CH_3CN, vs Ag/AgCl): $E_{1/2}$ = −0.33 V.

X-ray crystallography: X-ray quality crystals were grown by slow diffusion of diethyl ether into acetonitrile solutions of complexes **2**, **3**, and **5**, and into an acetone solution of **4**. Data for the black crystals of **2**, **3**, and **4** were collected on a Nonius Kappa CCD diffractometer with graphite-monochromated $Mo_{K\alpha}$ radiation (λ = 0.71073 Å) at 233(2) K (**2**, **3**) and 243(2) K (**4**). Crystal data of **5** were collected on a Nonius CAD-4 diffractometer at 294(2) K.

Intensities were integrated using DENZO and scaled with SCALEPACK. Several scans in ϕ and ω directions were made to increase the number of redundant reflections, which were averaged in the refinement cycles. This procedure replaces an empirical absorption correction. The structure was solved with direct methods (SHELXS86) and refined against F^2 (SHELX97).[35] Hydrogen atoms at carbon atoms were added geometrically and refined using a riding model, hydrogen atoms of the water molecules were refined regular with isotropic displacement parameters. All non-hydrogen atoms were refined with anisotropic displacement parameters.

Further details of the crystal structure determinations are given in Table 1. Graphical representations were obtained with ORTEPIII,[36] SHELX97, and Mercury 1.1 (CCDC) programs. CCDC-215903 (**2**), CCDC-215904 (**3**), CCDC-215905 (**4**), and CCDC-215906 (**5**) contain the supplementary crystallographic data for this paper. These data can be obtained free of charge via www.ccdc.cam.ac.uk/conts/retrieving.html (or from the Cambridge Crystallographic Data Centre, 12 Union Road, Cambridge CB21EZ, UK; fax: (+44) 1223-336-033; or deposit@ccdc.cam.uk).

Methods of calculation: The structures of dianionic $[Cu(pds)_2]^{2-}$, monoanionic $[Cu(pdt)_2]^-$ and $[Cu(pds)_2]^-$, and neutral $[Cu(pds)_2]$ units were optimized by DFT calculations with the B3LYP hybrid functional[37–39] with a triple-ξ basis set proposed by Schaefer et al.[40] including polarization functions for all atoms. The calculations were performed with the Gaussian 98 code (Revision A.11)[41] on starting orbitals provided by Jaguar 4.1 code.[42] The structural optimizations were performed with no restrictions on the geometry. The stability of the wavefunction for the singlet states of $[Cu(pds)_2]^-$ and $[Cu(pdt)_2]^-$ was verified by using the option stable = opt with the Gaussian 98 code. The time-dependent DFT calculations[43,44] including solvent effects with the conductor polarizable calculation model (CPCM)[45] to simulate the acetonitrile solvent were performed with Gaussian 03 code (Revision B.04).[46] In such calculations, a reoptimization of the geometries including the solvent effect was carried out.

Acknowledgements

This work was supported by grants from DGI Spain (Project BQU2000-1157), DGR Catalonia (Project 2000SGR00114), and FCT Portugal (Contract POCTI/35342/QUI/2000). The collaboration between the authors from Barcelona and Sacavém was supported by the ICCT-CSIC bilateral agreement and benefited also from COST action D14. The authors thank E. B. Lopes for electrical conductivity measurements.

[1] a) A. E. Underhill, M. M. Ahmad, *J. Chem. Soc. Chem. Commun.* **1981**, 67; b) A. E. Underhill, P. I. Clemenson, M. B. Hursthouse, R. L. Short, G. J. Ashwell, I. M. Sandy, K. Carneiro, *Synth. Met.* **1987**, *19*, 953.
[2] a) P. Cassoux, L. Valade, H. Kobayashi, A. Kobayashi, R. A. Clark, A. E. Underhill, *Coord. Chem. Rev.* **1991**, *110*, 115; b) P. Cassoux, J. S. Miller in *Chemistry of Advanced Materials* (Eds.: L. V. Interrante, M. J. Hampden-Smith), Wiley, New York, **1998**, pp. 19–72; c) R. Kato, Y. Kashimura, S. Aonuma, N. Hanasaki, H. Tajima, *Solid State Commun.* **1998**, *105(9)*, 561–565.
[3] R. E. Peierls, *Quantum Theory of Solids*; Oxford University Press, **1955**, p. 108.
[4] a) H. Kobayashi, H. Tomita, T. Naito, A. Kobayashi, F. Sakai, T. Watanabe, P. Cassoux, *J. Am. Chem. Soc.* **1996**, *118*, 368–377; b) T. Courcet, I. Malfant, K. Pokhodonia, P. Cassoux, *New. J. Chem.* **1998**, 585–589; c) H. Fujiwara, E. Ojima, H. Kobayashi, T. Courcet, I. Malfant, P. Cassoux, *Eur. J. Inorg. Chem.* **1998**, 1631–1639.
[5] N. J. Harris, A. E. Underhill, *J. Chem. Soc. Dalton Trans.* **1987**, 1683–1685.
[6] H. H. Wang, S. B. Fox, E. B. Yagubskii, L. A. Kushch, A. I. Kotov, M.-H. Whangbo, *J. Am. Chem. Soc.* **1997**, *119*, 7601–7602.
[7] D. Herebian, E. Bothe, F. Neese, T. Weyhermüller, K. Wieghardt, *J. Am. Chem. Soc.* **2003**, *125*, 9116–9128.
[8] a) C. G. Pierpont, C. W. Lange, *Prog. Inorg. Chem.* **1994**, *41*, 331.
[9] A. Mederos, S. Domiguez, R. Hernandez-Molina, J. Sanchiz, F. Brito, *Coord. Chem. Rev.* **1999**, *193–195*, 913.
[10] J. A. McCleverty, *Prog. Inorg. Chem.* **1968**, *10*, 49.
[11] R. H. Holm, M. J. Olanov, *Prog. Inorg. Chem.* **1971**, *14*, 241.
[12] P. Chaudhuri, C. N. Verani, E. Bill, E. Bothe, T. Weyhermüller, K. Wieghardt, *J. Am. Chem. Soc.* **2001**, *123*, 2213.
[13] C. N. Verani, S. Gallert, E. Bill, T. Weyhermüller, K. Wieghardt, P. Chaudhuri, *Chem. Commun.* **1999**, 1474.
[14] H. Chun, C. N. Verani, P. Chaudhuri, E. Bothe, T. Weyhermüller, K. Wieghardt, *Inorg. Chem.* **2001**, *40*, 4157.
[15] H. Chun, T. Weyhermüller, E. Bill, K. Wieghardt, *Angew. Chem.* **2001**, *113*, 2552–2555; *Angew. Chem. Int. Ed.* **2001**, *40*, 2489–2492.
[16] D. Herebian, E. Bothe, E. Bill, T. Weyhermüller, K. Wieghardt, *J. Am. Chem. Soc.* **2001**, *123*, 10012.
[17] C.-H. Hsieh, I-J. Hsu, C.-M. Lee, S.-C. Ke, T.-Y. Wang, G.-H. Lee, Y. Wang, J.-M. Chen, J.-F. Lee, W.-F. Liaw, *Inorg. Chem.* **2003**, *42*, 3925.
[18] a) G. C. Papavassiliou, S. Y. Yiannopoulos, J. S. Zambounis, *Chem. Soc.* **1987**, *27*, 265–268; b) J. Morgado, M. T. Duarte, L. Alcácer, I. C. Santos, R. T. Henriques, M. Almeida, *Synth. Met.* **1997**, *86*, 2187–2188.
[19] X. Ribas, J. Dias, J. Morgado, K. Wurst, M. Almeida, J. Veciana, C. Rovira, *Cryst. Eng. Commun.* **2002**, *4*, 564–567.
[20] J. J. Novoa, M. C. Rovira, C. Rovira, J. Veciana, J. Tarrés, *Adv. Mater.* **1995**, *7*, 223–227.
[21] a) G. R. Desiraju, *Acc. Chem. Res.* **2002**, *35*, 565–573; b) T. Steiner, *Angew. Chem.* **2002**, *114*, 50–80; *Angew. Chem. Int. Ed.*, **2002**, *41*, 48–76; c) G. A. Jeffrey, *An Introduction to Hydrogen Bonding*, Oxford University Press, Oxford, **1997**.
[22] a) M. Melnik, M. Kabesova, *J. Coord. Chem.* **2000**, *50*, 323–338; b) X. Ribas, D. A. Jackson, B. Donnadieu, J. Mahía, T. Parella, R. Xifra, B. Hedman, K. O. Hodgson, A. Llobet, T. D. P. Stack, *Angew. Chem.* **2002**, *114*, 3117–3120; *Angew. Chem. Int. Ed.* **2002**, *41*, 2991–2994.
[23] G. Speier, V. Fülöp, *J. Chem. Soc. Chem. Commun.* **1990**, 905.
[24] a) C. Krebs, T. Glaser, E. Bill, T. Weyhermüller, W. Meyer-Klaucke, K. Wieghardt, *Angew. Chem.* **1999**, *111*, 370–372; *Angew. Chem. Int. Ed.* **1999**, *38*, 359–361; b) F. A. Cotton, G. Wilkinson, *Advanced Inorganic Chemistry*, 5th ed., Wiley, New York, **1988**, p. 774.
[25] V. Bachler, G. Olbrich, F. Neese, K. Wieghardt, *Inorg. Chem.* **2002**, *41*, 4179.
[26] D. Sellmann, M. Gecj, F. Knoch, G. Ritter, J. Dengler, *J. Am. Chem. Soc.* **1991**, *113*, 3819.
[27] R. J. Batchelor, F. W. B. Einstein, I. D. Gay, J.-H. Gu, S. Mehta, B. M. Pinto, X.-M. Zhou, *Inorg. Chem.* **2000**, *39*, 2558–2571.
[28] H. Tanaka, H. Kobayashi, A. Kobayashi, *J. Am. Chem. Soc.* **2002**, *124*, 10002–10003.
[29] The TBA complex $[Ni^{III}(pds)_2]$ exhibits an Ni^{II}/Ni^{III} redox potential at $E_{1/2} = -0.16$ V, C. Rovira et al. unpublished results.
[30] R. K. Szilagyi, B. S. Lim, T. Glaser, R. H. Holm, B. Hedman, K. O. Hodgson, E. I. Solomon, *J. Am. Chem. Soc.* **2003**, *125*, 9158–9169.
[31] W. Kutzelnigg, *Angew. Chem.* **1984**, *96*, 262; *Angew. Chem. Int. Ed. Engl.* **1984**, *23*, 272.
[32] G. A. Zvereva, G. M. Larin, *Russ. J. Coord. Chem.* **1998**, *24*, 712–714.
[33] J. L. DuBois, P. Mukherjee, T. D, P. Stack, B. Hedman, E. I. Solomon, K. O. Hodgson, *J. Am. Chem. Soc.* **2000**, *122*, 5775–8787.
[34] a) C. Rovira, *Chem. Eur. J.* **2000**, *6*, 1723–1729; b) C. Rovira, J. Veciana, E. Ribera, J. Tarrés, E. Canadell, R. Rousseau, M. Mas, E. Molins, M. Almeida, R. T. Henriques, J. Morgado, J.-P. Schoeffel, J.-P. Pouget, *Angew. Chem.* **1997**, *109*, 2417–2421; *Angew. Chem. Int. Ed. Engl.* **1997**, *36*, 2418–2421.
[35] G. M. Sheldrick, SHELXL97: Program for the refinement of crystal structures, University of Göttingen, Germany, **1997**.
[36] P. McArdle, *J. Appl. Crystallogr.* **1995**, *28*, 65.
[37] A. D. Becke, *Phys. Rev. A* **1988**, *38*, 3098.
[38] A. D. Becke, *J. Chem. Phys.* **1993**, *98*, 5648.
[39] C. Lee, W. Yang, R. G. Parr, *Phys. Rev. [Sect.] B* **1988**, *37*, 785.
[40] A. Schaefer, C. Huber, R. Ahlrichs, *J. Chem. Phys.* **1994**, *100*, 5829.
[41] Gaussian 98, Revision A.11, M. J. Frisch, G. W. Trucks, H. B. Schlegel, G. E. Scuseria, M. A. Robb, J. R. Cheeseman, V. G. Zakrzewski, J. A. Montgomery, R. E. Stratmann, J. C. Burant, S. Dapprich, J. M. Millam, A. D. Daniels, K. N. Kudin, M. C. Strain, O. Farkas, J. Tomasi, V. Barone, M. Cossi, R. Cammi, B. Mennucci, C. Pomelli, C. Adamo, S. Clifford, J. Ochterski, G. A. Petersson, P. Y. Ayala, Q. Cui, K. Morokuma, D. K. Malick, A. D. Rabuck, K. Raghavachari, J. B. Foresman, J. Cioslowski, J. V. Ortiz, B. B. Stefanov, G. Liu, A. Liashenko, P. Piskorz, I. Komaromi, R. Gomperts, R. L. Martin, D. J. Fox, T. Keith, M. A. Al-Laham, C. Y. Peng, A. Nanayakkara, C. Gonzalez, M. Challacombe, P. M. W. Gill, B. G. Johnson, W. Chen, M. W. Wong, J. L. Andres, M. Head-Gordon, E. S. Replogle, J. A. Pople, Gaussian, Inc, Pittsburgh, PA, **1998**.
[42] Jaguar 4.1, Schrödinger, Inc., Portland, **2000**.
[43] M. E. Casida, C. Jamorski, K. C. Casida, D. R. Salahub, *J. Chem. Phys.* **1998**, *108*, 4439.
[44] R. E. Stratmann, G. E. Scuseria, M. J. Frisch, *J. Chem. Phys.* **1998**, *109*, 8218.
[45] V. Barone, M. Cossi, *J. Phys. Chem. A* **1998**, *102*, 1995.
[46] Gaussian 03, Revision B.04, M. J. Frisch, G. W. Trucks, H. B. Schlegel, G. E. Scuseria, M. A. Robb, J. R. Cheeseman, J. A. Montgomery, T. Vreven, K. N. Kudin, J. C. Burant, J. M. Millam, S. S. Iyengar, J.

Tomasi, V. Barone, B. Mennucci, M. Cossi, G. Scalmani, N. Rega, G. A. Petersson, H. Nakatsuji, M. Hada, M. Ehara, K. Toyota, R. Fukuda, J. Hasegawa, H. Ishida, T. Nakajima, Y. Honda, O. Kitao, H. Nakai, M. Klene, X. Li, J. E. Knox, H. P. Hratchian, J. B. Cross, C. Adamo, J. Jaramillo, R. Gomperts, R. E. Stratmann, O. Yazyev, A. J. Austin, R. Cammi, C. Pomelli, J. Ochterski, P. Y. Ayala, K. Morokuma, G. A. Voth, P. Salvador, J. J. Dannenberg, V. G. Zakrzewski, S. Dapprich, A. D. Daniels, M. C. Strain, O. Farkas, D. K. Malick, A. D. Rabuck, K. Raghavachari, J. B. Foresman, J. V. Ortiz, Q. Cui, A. G. Baboul, S. Clifford, J. Cioslowski, B. B. Stefanov, G. Liu, A. Liashenko, P. Piskorz, I. Komaromi, R. L. Martin, D. J. Fox, T. Keith, M. A. Al-Laham, C. Y. Peng, A. Nanayakkara, M. Challacombe, P. M. W. Gill, B. Johnson, W. Chen, M. W. Wong, C. Gonzalez, J. A. Pople, Gaussian, Inc, Pittsburgh, PA, **2003**.

Received: August 1, 2003
Revised: December 5, 2003 [F5422]